Atmos. Chem. Phys. Discuss., 10, 29897–29922, 2010
www.atmos-chem-phys-discuss.net/10/29897/2010/
doi:10.5194/acpd-10-29897-2010
© Author(s) 2010. CC Attribution 3.0 License.

Atmospheric Chemistry and Physics Discussions

This discussion paper is/has been under review for the journal Atmospheric Chemistry and Physics (ACP). Please refer to the corresponding final paper in ACP if available.

Investigating potential biases in observed and modeled metrics of aerosol-cloud-precipitation interactions

H. T. Duong[1], **A. Sorooshian**[1,2], **and G. Feingold**[3]

[1]Department of Chemical and Environmental Engineering, University of Arizona, Tucson, Arizona 85721, USA
[2]Department of Atmospheric Sciences, University of Arizona, Tucson, Arizona 85721, USA
[3]NOAA Earth Systems Research Laboratory, Boulder, Colorado 80305, USA

Received: 29 October 2010 – Accepted: 23 November 2010 – Published: 8 December 2010

Correspondence to: A. Sorooshian (armin@email.arizona.edu)

Published by Copernicus Publications on behalf of the European Geosciences Union.

Abstract

This study utilizes large eddy simulation, aircraft measurements, and satellite observations to identify factors that bias the absolute magnitude of metrics of aerosol-cloud-precipitation interactions for warm clouds. The metrics considered are precipitation susceptibility S_o, which examines rain rate sensitivity to changes in drop number, and a cloud-precipitation metric, χ, which relates changes in rain rate to those in drop size. While wide ranges in rain rate exist at fixed cloud drop concentration for different cloud liquid water amounts, χ and S_o are shown to be relatively insensitive to the growth phase of the cloud for large datasets that include data representing the full spectrum of cloud lifetime. Spatial resolution of measurements is shown to influence both the magnitude and liquid water path-dependent behavior of S_o and χ. Other factors of importance are the choice of how to quantify rain rate, drop size, and the cloud condensation nucleus proxy. Finally, low biases in retrieved aerosol amounts owing to wet scavenging and high biases associated with above-cloud aerosol layers should be accounted for. The paper explores the impact of these effects for model, satellite, and aircraft data.

1 Introduction

The representation of the physical processes relating aerosol particles, clouds, and precipitation in general circulation models (GCMs) is characterized by highly uncertain parameterizations (Lohmann and Feichter, 2005). The links between aerosol, clouds, and rainfall remain poorly understood owing to the complexity of the processes, measurement limitations, and the difficulty in isolating aerosol effects from competing factors such as meteorology. Climate models employ spatial resolution (>100 km) that is far coarser than the tools used to inform parameterizations of aerosol-cloud processes, including cloud model simulations and observations. Even at the higher spatial resolutions available with these techniques, there exists large uncertainty in quantifying cloud

ACPD
10, 29897–29922, 2010

responses to changes in aerosol owing to differences in measurement and data analysis techniques (McComiskey and Feingold, 2008; Grandey and Stier, 2010). It is therefore important to address the source of variability in reported values of aerosol-cloud-precipitation metrics, especially when comparing measurements from in-situ measurements, models, and satellite remote sensors.

The various constructs that are examined in this work are of interest because they provide a link between climate model parameterizations and observational and modeling studies. For example, the process of collision-coalescence between cloud drops to form precipitation, termed autoconversion, is represented in GCMs using a parameterization typically relating rain rate (R) to the amount of liquid water in clouds (i.e. liquid water path, LWP) and drop number concentration (N_d) in the form of the following power law:

$$R \sim \mathrm{LWP}^{x_1} N_d^{x_2} \tag{1}$$

The connection between aerosol and R is contained within the x_2 term since N_d is directly proportional to aerosol number concentration, N_a. Values of x_2 range widely between −0.8 and −1.75 based on numerous aircraft-based studies in stratocumulus regions (Pawlowska and Brenguier, 2003; Comstock et al., 2004; van Zanten et al., 2005; Wood, 2005; Lu et al., 2009). Such a broad range leads to widely varying simulated strengths of the second aerosol indirect effect in climate models, some of which use x_2 values ranging between 0 and −1.79 (Quaas et al., 2009).

The following metrics have recently been introduced as a way to improve the quantification and understanding of aerosol-cloud-precipitation interactions (Feingold et al., 2001; Feingold and Siebert, 2009; Sorooshian et al., 2010):

$$\mathrm{ACI} = -\frac{\partial \ln r_e}{\partial \ln \alpha} \tag{2}$$

$$\chi = \frac{\partial \ln R}{\partial \ln r_e} \tag{3}$$

ACPD
10, 29897–29922, 2010

$$S_o = -\frac{d\ln R}{d\ln N_d} \quad (4a)$$

$$S'_o = -\frac{d\ln R}{d\ln \alpha} \quad (4b)$$

where r_e is drop effective radius, α is a cloud condensation nuclei (CCN) proxy, and all partial derivatives are evaluated with macrophysical conditions (e.g. LWP) held fixed. ACI relates a change in drop size to an aerosol perturbation, and using basic assumptions, this term is bounded by the range 0–0.33; a value of 0.33 corresponds to complete activation of sub-cloud aerosol into droplets (i.e. α=N_d). A wide range of ACI values has been reported in the literature, with higher values usually associated with in-situ and ground-based measurements as compared to satellite remote sensing observations (McComiskey and Feingold, 2008); this study showed that a wide range of radiative forcing estimates (from −3 to −10 W m^{-2}) can result simply from a difference in ACI of 0.05.

The relationship between aerosol perturbations and rain rate can be quantified as the precipitation susceptibility (S_o), which relates the precipitation response to a change in drop concentration. Alternatively, S_o can be indirectly obtained by the product of ACI and χ (Sorooshian et al., 2010). Unlike Eq. (4a), the form of the susceptibility in Eq. (4b) can be quantified using satellite data since N_d can only be inferred from space with assumptions, whereas α (in the form of aerosol optical depth or aerosol index) can be more easily measured. Precipitation susceptibility is useful in that it comprises variables that can be observed and it is directly related to the previously-defined x_2 value in the autoconversion parameterization employed in climate models (at fixed LWP, S_o=−x_2).

A number of recent studies have shown similar qualitative behavior of S_o as a function of LWP for shallow cumulus clouds (Jiang et al., 2010; Sorooshian et al., 2009, 2010), where at low LWP, clouds are relatively insensitive to aerosol as they do not have a great potential to precipitate, while at larger LWP, clouds can precipitate more

ACPD
10, 29897–29922, 2010

and they become progressively more sensitive to aerosol perturbations. The precipitation susceptibility of warm clouds grows with increasing LWP to a maximum, after which it decreases. This represents a shift from a precipitation regime dominated by autoconversion to one of accretion. Sorooshian et al. (2010) showed using modeling and observational data that χ essentially captures the essence of S_o behavior as a function of LWP, while ACI is approximately invariant with LWP, provided data has been binned by LWP. However, these studies highlighted a number of issues, including statistical insignificance of the values of these metrics when calculated using satellite data (S_o'), and disagreement in both the absolute values of these metrics, and their LWP-dependent behavior amongst the various methods (in-situ measurements, models, satellite remote sensing).

The goal of this study is to directly identify the sources of disagreement in ACI, χ, S_o between satellite observations, in-situ observations, and large eddy simulation. We do so by examining the sensitivity of these parameters to a number of factors thought to bias their absolute magnitudes and LWP-dependent behavior. Only warm clouds are considered. The paper is structured as follows: (i) overview of experimental methods; (ii) analysis of the sensitivity of aerosol-cloud-precipitation metrics to cloud lifetime and spatial resolution of measurements, method of quantifying aerosol-cloud parameters, using artificially low and high retrieved aerosol concentrations owing to wet scavenging and above-cloud aerosol layers, respectively; and (iii) conclusions.

2 Experimental methods

2.1 Modeling

The model used in this work is the Regional Atmospheric Modeling System (RAMS, version 6.0) (Cotton et al., 2003), a large eddy simulation (LES) model, coupled to an explicit bin-resolving microphysical model (Feingold et al., 1996; Stevens et al., 1996). The simulations are initialized with a thermodynamic sounding based on data from the

ACPD
10, 29897–29922, 2010

Rain In Cumulus over Ocean (RICO) field experiment (Jiang et al., 2009, 2010); the model domain size is 25.6 km×25.6 km×6 km with a horizontal grid spacing of 100 m and vertical grid spacing of Δz=40 m up to 4 km, and vertically stretched above that height with a stretch factor of 1.035. The analysis is restricted to clouds that exhibit lifetimes between 15–45 min. Extensive details on lifetime and areal extent statistics for the entire cloud population are provided by Jiang et al. (2010).

Two simulations were carried out with initial aerosol concentrations (N_a) of 100 cm^{-3} and 300 cm^{-3} to represent clean and moderately polluted clouds, respectively. The simulations were run for 12 h, but only output from hours 6 and 7 were examined. Individual clouds were manually tracked over the course of their lifetime, where a cloud is defined as having an average LWP exceeding 20 g m^{-2} and a minimum size of 0.3 km×0.3 km. Merging and non-precipitating clouds (R<0.5 mm day^{-1}) are excluded in the analysis. At each minute of a cloud's life the maximum cloud drop concentration ($N_{d,max}$), LWP, maximum drop effective radius ($r_{e,max}$), cloud-top drop effective radius ($r_{e,top}$), and maximum precipitation rate (R_{max}) are calculated. These values are then averaged over three different spatial resolutions (0.3 km×0.3 km, 0.5 km×0.5 km, and 0.7 km×0.7 km) at each sampling time. Note that some clouds were not sufficiently large to allow averages over the larger spatial domains. Clouds are categorized into three regimes based on terciles of lifetime: beginning (0–33% lifetime), middle (33–67% lifetime) and end (67–100% lifetime). ACI, χ, and S_o are quantified in each cloud lifetime category for 15 different LWP bins with midpoints including 50 g m^{-2}, 100 g m^{-2}, and up to 1400 g m^{-2} in 100 g m^{-2} increments. LWP bins extend up to 10% around the midpoints (i.e. LWP±10%×LWP) to maintain similar numbers of points in each bin.

2.2 Aircraft measurements

The aircraft measurements derive from the second Marine Stratus/Stratocumulus Experiment (MASE-II) field campaign during July 2007 off the coast of Monterey, California. The objective of MASE-II was to study aerosol-cloud interactions in stratocumulus

ACPD
10, 29897–29922, 2010

clouds. The flights paths were designed to fly level legs below cloud base, at three levels in cloud (above-base, mid-level, below-top), and above cloud. Seven flights are examined here. The measurements and instrument payload are described extensively elsewhere (Hersey et al., 2009). Briefly, the forward scattering spectrometer probe (FSSP; PMS, modified by DMT Inc.) was used to quantify N_d and r_e, while the cloud imaging probe (CIP), part of the cloud/aerosol/precipitation spectrometer package (CAPS; DMT Inc), was used to quantify drizzle rate (R). Maximum values for N_d, r_e, and R were calculated in cloud from the maximum values of each variable over a 2.5 km long stretch of a level leg, which usually lasted 10–15 min (30–45 km at the aircraft speed ~50 m s^{-1}). Cloud-top and cloud-base values of various parameters were obtained by averaging data over the entire below-top and above-base legs, respectively. LWP is quantified as the vertical integration of the liquid water content measured by a PVM-100 probe (Gerber et al., 1994). Data used in calculation of cloud parameters were only taken when LWC exceeded 0.05 g m^{-3} to avoid biased calculations when breaks appeared in the otherwise solid cloud. A condensation particle counter (TSI CPC 3010, $D_p \geq 10$ nm) and a passive cavity aerosol spectrometer probe (PCASP; PMS; $D_p \simeq 100$ nm to 2.6 µm) were used to quantify the sub-cloud aerosol number concentration (N_a).

2.3 Satellite products

For this study, 27 months of data are used from NASA's A Train constellation of satellites beginning from June 2006. The description of all satellite products and data filtering methodology are described extensively elsewhere (Lebsock et al., 2008; Sorooshian et al., 2010). Briefly, data are only used for warm maritime clouds in conditions of single cloud layers. Precipitation rate data are obtained from the CloudSat cloud profiling radar (CPR) (2C-PRECIP-COLUMN product; Haynes et al., 2009) within the range of 0.1–5 mm h^{-1}. Collocated aerosol data are obtained from the Moderate Resolution Imaging Spectroradiometer (MODIS), specifically the 1°×1° gridded aerosol index (Level 3, MODIS Collection 5) (Remer et al., 2005), which is defined as

ACPD
10, 29897–29922, 2010

the product of the 0.55 µm aerosol optical depth×0.55/0.867 µm Ångstrom exponent. AI serves as a sub-cloud CCN proxy in the analysis. Level 2 MODIS products at 1-km resolution are used to obtain data for cloud-top drop effective radius (r_e) and LWP (Platnick et al., 2003). In addition, estimates of the lower tropospheric static stability (LTSS) from the European Centre for Medium Range Weather Forecasts (ECMWF) analyses that have been matched to the CloudSat footprint (Partain, 2007) are used to quantify atmospheric stability.

3 Results and discussion

Large eddy simulation output is used in Sects. 3.1 and 3.2 to examine the importance of cloud lifetime and spatial resolution. Aircraft measurements are used in Sect. 3.3 to discuss the choice of how to quantify aerosol-cloud properties. Satellite data are used in Sects. 3.4 and 3.5 to look at the effect of above-cloud aerosol layers and wet scavenging, respectively.

3.1 Cloud lifetime

Recent work has attempted to parameterize shallow cumulus R in terms of N_d and LWP (Jiang et al., 2010). That work showed that the parameterization is significantly improved when cloud lifetime is taken into account. Building on those results, we quantify the sensitivity of χ and S_o to cloud lifetime for shallow cumulus clouds using LES output. Modeling is used for this effort since satellites provide "snapshots" at one point in time of a cloud field and therefore there is no direct measurement of what stage of a cloud the retrieved data represent. For example, is a cloud with a LWP of 800 g m^{-2} a budding cloud that is in a growing stage or a decaying cloud that is being depleted of its liquid water via precipitation?

To determine what effect cloud lifetime will have on S_o and χ, the dynamic ranges of R and r_e are first evaluated at a representative LWP value (800 g m^{-2}) for

ACPD
10, 29897–29922, 2010

a population of clean and polluted clouds at all stages of their lifetime between 0–100% (Fig. 1). Note that few points are available at the beginning stages of clouds as they have not yet had sufficient time to reach a LWP of 800 g m^{-2}. The two clusters of points at varying levels of N_d correspond to the "clean" and "polluted" simulations. Precipitation is driven more directly by droplet size rather than N_d, which explains the narrower range in R at fixed r_e as compared to fixed N_d (i.e. R and r_e are more closely linked physically than R and N_d). Cloud lifetime is shown to be responsible for the wide range in R at fixed N_d, where clouds near the end of their lifetime are raining most heavily. The dynamic range in R tends to be wider for the clean clouds versus more polluted clouds since they have a greater potential to rain owing to larger droplets at fixed LWP.

Figure 2 illustrates the effect of cloud lifetime on the values of χ and S_o as a function of LWP when evaluated at different spatial resolutions. Consistent with previous work, χ and S_o are non-monotonic functions of LWP and similarly exhibit small values at low LWP and then increase up to a threshold LWP value after which they decrease. At fixed spatial resolution, the absolute values and LWP-dependent behavior of χ and S_o are insensitive to whether those values were quantified at lifetimes of 0–33%, 33–67%, 67–100%, or 0–100%. From Fig. 1, it is evident that the rare case when lifetime may have an important impact on S_o is when using small datasets that only include clouds in clean and dirty conditions that were at opposite ends of cloud lifetime (clean+growing vs. dirty+decaying; clean+decaying vs. dirty+growing). χ will be less sensitive to lifetime as there is a relatively small dynamic range in R at a given r_e as compared to fixed N_d conditions.

Remote sensing datasets typically include high volumes of data, so within a particular LWP bin it is expected that clouds across a wide range of lifetimes will be represented. Since the results for ACI (not shown), χ, and S_o are similar for clouds when analyzing data for various bins of cloud lifetime (0–33%, 33–67%, 67–100%, and 0–100%), this suggests that when using large datasets the absolute values of ACI, χ, and S_o will not be biased to a large extent. The effect of lifetime will likely become more

ACPD
10, 29897–29922, 2010

important when using small datasets.

3.2 Spatial resolution

An important feature of the LES results in Fig. 2 is the effect of spatial resolution on the LWP-dependent behavior of χ and S_o. As the spatial resolution decreases, the peak values of χ and S_o shift to lower LWP values. Therefore, the choice of lower spatial resolution (i.e. 0.7 km×0.7 km versus 0.3 km×0.3 km) has the effect of compressing the χ–LWP and S_o–LWP curves to lower LWP values while still maintaining similar absolute values of χ and S_o. This effect of spatial resolution can now explain results in recent studies (Jiang et al., 2010; Sorooshian et al., 2010) where the precipitation susceptibility of clouds was shown to exhibit a maximum at varying LWPs, owing to quantifying LWP across different spatial scales. Although not shown, ACI is insensitive to the choice of spatial resolution since it is relatively constant as a function of LWP regardless of the size of the spatial resolution. In general, χ and S_o will likely exhibit peak values at lower LWP for satellite data (as compared to models and in-situ measurements) where LWP is averaged over larger spatial scales typically exceeding 1 km.

3.3 Method of quantifying aerosol-cloud properties

The following analysis assesses the sensitivity of ACI, χ, and, S_o to the choice of how one quantifies the sub-components of these metrics (r_e, N_d, and R) using aircraft measurements from the MASE II study. As an example of why this is important, the choice of whether to use cloud column-integrated values of r_e versus those at cloud-top has previously been shown to influence the value of ACI (Masunaga et al., 2002; Matsui et al., 2004, 2006). Data from seven total cloud cases are examined exhibiting a LWP range between 31–55 g m^{-2} and an average sub-cloud N_a range between 180–1400 cm^{-3} (using CPC 3010). Cloud base drizzle rates during these cases ranged between 0.5–2.7 mm day^{-1}. While the value of r_e is retrieved with satellite remote

ACPD
10, 29897–29922, 2010

sensors at cloud-top, the aircraft data are used to quantify this parameter in multiple ways including at cloud-top, the maximum in-cloud value, and a column-integrated average. The sub-cloud leg-mean N_a value is quantified using a CPC 3010 and a PCASP, while N_d is quantified as a maximum in-cloud value and a column-integrated in-cloud value. In addition to column-integrated and maximum values, R is quantified here as the leg-mean value above cloud base.

Table 1 shows that ACI values are smaller than $-\frac{\partial \ln r_e}{\partial \ln N_d}\Big|_{LWP}$ (=ACI with N_d in denominator), with slight enhancements in ACI when using N_a values from the PCASP as compared to the CPC 3010. ACI values are expected to be lower than $-\frac{\partial \ln r_e}{\partial \ln N_d}\Big|_{LWP}$, with a reduction approximately equal to the factor "c": $N_d \sim N_a^c$ (Feingold et al., 2001). The values of "c" for these seven cases when using N_a (from CPC and PCASP) and $N_{d,max}$ are 0.62 and 0.67, respectively, which are close to the ratios of ACI when calculated using N_a as the CCN proxy as compared to $N_{d,max}$ (0.67–0.76). The $-\frac{\partial \ln r_e}{\partial \ln N_d}\Big|_{LWP}$ values tend to approach 0.33 when using the N_d and r_e combinations that exhibit the widest range of values (value range: $N_{d,max} > N_{d,col}$ and $r_{e,max} > r_{e,top} > r_{e,col}$). Similar reasoning explains why values of χ and S_o (or S_o') are significantly greater when using R_{max} versus either R_{base} or R_{col}. These results are consistent with recent work that showed larger values of ACI for wider ranges of AI (all else fixed) using satellite remote sensing data (Sorooshian and Duong, 2010).

Why are the values in Table 1 greatest when quantifying the respective subcomponents in ways that maximize their dynamic range? The strength of the relationship between an aerosol perturbation and drop size (or R) at fixed LWP is thought to be more pronounced when quantifying maximum values of N_d and r_e (or R) rather than leg-averaged values that may average out and obfuscate the desired signal. To provide further support for this explanation, Fig. 3 summarizes the dependence of the parameters on the level flight leg length over which data were collected (centered around maximum drop effective radius). It is shown that the maximum values occur at the smallest leg-lengths (<3 km) and level off when the data are averaged over larger spatial scales.

ACPD
10, 29897–29922, 2010

It is also worth noting that the product of ACI and χ agrees with the directly-quantified S_o; for example, the product of χ (using $r_{e,max}$ and the various rain rates) with 0.31 (=ACI with $r_{e,max}$ and $N_{d,max}$) agrees to within 9% for all three combinations. This provides additional support for the utility of the deconstruction of the S_o metric into sub-components (Sorooshian et al., 2010) to improve confidence in causal relationships between aerosol perturbations and the precipitation response of warm clouds by quantifying an intermediate step with the use of r_e (or alternatively cloud optical depth). Past work has also highlighted the significance of the relationship between drop effective radius and precipitation (e.g., Rosenfeld and Gutman, 1994).

3.4 Above-cloud aerosol layers

Previous work attempted to identify warm oceanic regions between a latitude range of $\pm 30^{\circ}$ with the largest S_o (Sorooshian et al., 2009) and the largest potential relative reductions in R. It was shown, using a simplified approach, that the greatest predicted relative reduction in warm rainfall is off the western coast of Africa; it is noted that this region did not exhibit the greatest absolute reduction simply because the precipitation rates in that region are low. In that work, ΔR was calculated as the product of annual average of daily S_o values (as determined by satellite-retrieved LWP and the S_o–LWP relationship from LES output for warm clouds) and $d\ln(\mathrm{AI})$, as calculated from the dispersion (standard deviation/mean) in aerosol index for 2007. However, the assumption that a column-integrated value of AI is representative of aerosol impacting a cloud is especially problematic in conditions characterized by high above-cloud aerosol concentrations. In these conditions, AI becomes a poor proxy for sub-cloud CCN. Such aerosol plumes, which are common during the biomass burning season off the west coast of Africa, are clearly evident based on CALIPSO observations (e.g., Chand et al., 2009).

A closer examination of this region off the coast of Africa is carried out to assess the sensitivity of ACI, χ, and S_o' to using satellite-retrieved aerosol in conditions when relatively high concentrations of aerosol reside above the cloud, to represent the sub-cloud

ACPD
10, 29897–29922, 2010

CCN concentration. The spatial domain of this case study is (5° N, 20° S; 5° E, 35° W) and the time duration is between June and October of 2006. CALIPSO is used to identify cases of above-cloud aerosol plumes during all A-Train overpasses when warm rain was evident based on CloudSat observations. MODIS aerosol data were then filtered to avoid any 1°×1° scenes containing the above-cloud aerosol plumes. The analysis of ACI, χ, and S_o' was subsequently carried out both with all of the data and with the filtered data. The analysis is conducted for 11 LWP bins with up to 10% spacing around bin midpoints, which increase in 25 g m^{-2} increments from 50 to 300 g m^{-2}. The clouds in this region typically exhibit LTSS values in excess of 20 °C, which is indicative of stratocumulus clouds. Caution was taken to use CloudSat data beginning vertically in the lowest clutter-free range gate above the surface, which is between 600 and 840 m (Haynes et al., 2009).

Figure 4a shows that filtering the above-cloud plume data results in an enhancement in the majority of ACI and S_o' points, which rely on the collocated aerosol data retrieved by MODIS. On average, the enhancement in ACI and S_o' was 20% and 156%, respectively, for the LWP range examined. The explanation for the depression of these values during cases of above-cloud plumes likely stems from a cluster of data points at very high aerosol concentrations that obfuscate the desired ACI and S_o' signals (hypothetically illustrated in Fig. 5), leading to a reduction in their absolute values. Above-cloud aerosol layers present a factor that may lead to lower values of ACI and S_o' as compared to surface and aircraft measurements and cloud models that are immune to this issue. The values of χ tend to be more evenly scattered about the 1:1 line, which is partly expected as χ does not rely on collocated aerosol data and thus is less sensitive to above-cloud plumes. On average, there was an 8% enhancement in χ after the data filtering.

An issue that cannot be ignored in this discussion is the effect of overlaying aerosol layers on MODIS retrievals of cloud properties such as r_e and LWP, which are typically thought to be biased low (e.g., Haywood et al., 2004; Cattani et al., 2006; Bennartz and Harshvardhan, 2007; Wilcox et al., 2009; Coddington et al., 2010). In support of

ACPD
10, 29897–29922, 2010

the presented analysis, potential biases in r_e have been shown to be less than 1 µm for retrievals where the visible reflectance is matched with the 3.7 µm or 2.13 µm reflectance. Wilcox et al. (2009) report that when the aerosol index obtained from the Ozone Monitoring Instrument (OMI) exceeds two, the estimated bias in the average LWP difference between AMSR-E and MODIS exceeds the instantaneous uncertainty in the retrievals. Even after removing the data points in this case study analysis that exceeded this OMI threshold value (to account for issues in LWP retrievals), the conclusions of this analysis remain robust.

3.5 Wet scavenging effects

Artificially low aerosol concentrations resulting from wet scavenging can also influence the values of ACI, χ, and S'_o. The methodology in a number of studies has included obtaining data for rain and cloud properties from CloudSat and MODIS with a spatial resolution on the order of 1 km, while aerosol data are retrieved from a significantly larger spatial domain (1°×1°) (Lebsock et al., 2008; Sorooshian et al., 2009, 2010). The effect of wet scavenging is tested using data for the months of June through August (JJA) between 2006–2008 and just the year 2007 within the tropics for shallow cumulus clouds. The Precipitation Estimation from Remotely Sensed Information using Artificial Neural Networks (PERSIANN; Sorooshian et al., 2000) product is used to remove cases of precipitation for a period of time up to a day before a satellite overpass within the same 1°×1° domain of MODIS aerosol retrievals. PERSIANN estimates rainfall using geostationary infrared imagery of clouds (e.g., GOES-8, GOES-9/10, GMS-5, Metsat-6/7) and microwave instantaneous rainfall estimates (e.g., TRMM TMI). The analysis is performed for 12 LWP bins with up to 10% spacing around bin midpoints, which include 50 g m^{-2}, 100 g m^{-2}, and up to 1100 g m^{-2} in 100 g m^{-2} increments. Approximately 20–40% of the points were removed in each LWP bin when accounting for the wet scavenging effect.

Figure 4b shows that ACI and S'_o values are scattered around the 1:1 line but with many points depressed after the PERSIANN filtering. The reduction in ACI and S'_o

ACPD
10, 29897–29922, 2010

as a result of the data filtering is likely due to aerosol measurements being biased low when wet scavenging is not taken into account. Because wet scavenging tends to influence the polluted scenes more than clean ones (because there is a greater potential to remove more aerosol; Fig. 5), larger aerosol values need to be shifted to commensurately larger values, which for the same cloud microphysical parameter results in weaker ACI/S_o' slopes. Similar to the analysis of artificially high aerosol levels in Sect. 3.3, the value of χ is less sensitive to the wet scavenging data filtering because it does not require aerosol data in its quantification.

4 Conclusions

In previous work we explored the use of various parameters (ACI, χ, and S_o, defined in Sect. 1) that attempt to quantify aerosol-cloud-precipitation processes, and here we assess the sensitivity of such metrics to numerous biasing factors using LES, satellite observations, and aircraft measurements. The major results of this work are as follows:

1. The time at which a cloud is sampled, relative to the overall cloud lifetime, could bias estimates of precipitation susceptibility because of the inherent timescale for a cloud to produce rainfall. This potential bias was examined for simulated shallow cumulus clouds. The absolute values of χ and S_o are insensitive to whether those values were quantified at the beginning, middle, or end of cloud lifetime, unless sampling conditions were to somehow be biased towards covariance between magnitude of the aerosol perturbation, and stage of cloud development. Such covariance would be unlikely to exist in nature, except perhaps in small datasets. In large datasets, such as those from satellites, the effects of lifetime will likely be small owing to averaging amongst vast amounts of data representing clouds at varying stages in their lifetime, at their instantaneously measured LWP.

2. The choice and/or limitation of spatial resolution in observational datasets are shown to influence the LWP-dependent behavior of χ and S_o. At low spatial resolution, the curves are compressed towards lower LWP (see Fig. 2); in other words, the point

ACPD
10, 29897–29922, 2010

at which the maximum values of χ and S_o are reached occur at lower LWPs. ACI is shown to be relatively constant as a function of LWP and therefore is not as dependent on spatial resolution as χ and S_o.

3. The absolute magnitudes of S_o, χ, and ACI are sensitive to the choice of how to quantify the aerosol proxy, r_e, and R (e.g., cloud-top, maximum, vertically-integrated), and to temporal/spatial averaging. Analyses of aircraft data of aerosol-stratocumulus interactions show that S_o, χ, and ACI are higher when using values of N_d, r_e, and R that exhibit the widest dynamic ranges over the span of clouds examined. This is most relevant to model and aircraft-based studies, where there are many choices for how to quantify these variable values, as opposed to satellite-based data sets where data products are more limited.

4. The inclusion of cases characterized by above-cloud aerosol plumes, as examined in a case study off the coast of western Africa, is shown to depress values of ACI and S'_o. This is explained by data points at very high aerosol concentrations that obfuscate the desired ACI and S'_o signals. Appropriate filtering of these instances shows more realistic sensitivity. On the other hand, accounting for low biases in retrieved aerosol amounts as a result of wet scavenging with the use of an artificial neural network algorithm is shown in some cases to result in lower values of ACI and S'_o. An explanation is that wet scavenging tends to influence the polluted scenes more than clean ones, resulting in greater reductions in aerosol abundance during cases with the lowest rain rates and drop sizes. The value of χ is relatively insensitive to both factors as it does not rely on collocated aerosol data, but only data within cloudy pixels.

While variations are expected in the values of the aerosol-cloud-rain constructs examined here owing to the complexity of these physical interactions and meteorological feedbacks, it is necessary to understand how much of the variability is due to differences in measurement/modeling methodologies and data analysis techniques. The results of this study point to the importance of considering all the issues identified above when comparing results with other independent studies examining aerosol-cloud interactions. For instance, details as basic as how, and at what resolution cloud

ACPD
10, 29897–29922, 2010

microphysical parameters are calculated may have a major impact on the absolute value of the precipitation susceptibility of clouds to aerosol particles. Of the various parameters relating aerosols to rain in this work, χ is shown to be the least sensitive to the biasing factors investigated as it does not require collocated aerosol data in its calculation, which is especially advantageous for satellite studies.

Acknowledgements. A.S. acknowledges support from an Office of Naval Research YIP Award (N00014-10-1-0811). The aircraft measurements were supported by the Office of Naval Research grant N00014-04-1-0018. G.F. acknowledges support from NOAA's Climate Goal.

References

Bennartz, R. and Harshvardhan: Correction to "Global assessment of marine boundary layer cloud droplet number concentration from satellite", J. Geophys. Res., 112, D16302, doi:10.1029/2007JD00884, 2007.

Cattani, E., Costa, M. J., Torricella, F., Levizzani, V., and Silva, A. M.: Influence of aerosol particles from biomass burning on cloud microphysical properties and radiative forcing, Atmos. Res., 82, 310–327, 2006.

Chand, D., Wood, R., Anderson, T., Satheesh, S. K., and Charlson, R. J.: Satellite-derived direct radiative effect of aerosols dependent on cloud cover, Nat. Geosci., 2, 181–184, 2009.

Coddington, O. M., Pilewskie, P., Redemann, J., Platnick, S., Russell, P. B., Schmidt, K. S., Gore, W. J., Livingston, J., Wind, G., and Vukicevic, T.: Examining the impact of overlying aerosols on the retrieval of cloud optical properties from passive remote sensing, J. Geophys. Res., 115, D10211, doi:10.1029/2009JD012829, 2010.

Comstock, K. K., Wood, R., Yuter, S. E., and Bretherton, C. S.: Reflectivity and rain rate in and below drizzling stratocumulus, Q. J. Roy. Meteor. Soc., 130, 2891–2918, 2004.

Cotton, W. R., Pielke, R. A., Walko, R. L., Liston, G. E., Tremback, C. J., Jiang, H., McAnelly, R. L., Harrington, J. Y., Nicholls, M. E., Carrio, G. G., and McFadden, J. P.: RAMS 2001: current status and future directions, Meteorol. Atmos. Phys., 82(1–4), 5–29, 2003.

Feingold, G. and Siebert, H.: In clouds in the perturbed climate system: their relationship to energy balance, atmospheric dynamics, and precipitation, in: Strüngmann Forum Reports,

ACPD

10, 29897–29922, 2010

2, edited by: Heintzenberg, J. and Charlson, R. J., The MIT Press, Cambridge, MA, 597 pp, 2009.
Feingold, G., Kreidenweis, S. M., Stevens, B., and Cotton, W. R.: Numerical simulations of stratocumulus processing of cloud condensation nuclei through collision-coalescence, J. Geophys. Res., 101(D16), 21391–21402, 1996.
Feingold, G., Remer, L. A., Ramaprasad, J., and Kaufman, Y. J.: Analysis of smoke impact on clouds in Brazilian biomass burning regions: an extension of Twomey's approach, J. Geophys. Res., 106, 22907–22922, 2001.
Gerber, H., Arends, B. G., and Ackerman, A. S.: New microphysics sensor for aircraft use, Atmos. Res., 31, 235–252, 1994.
Grandey, B. S. and Stier, P.: A critical look at spatial scale choices in satellite-based aerosol indirect effect studies, Atmos. Chem. Phys. Discuss., 10, 15417–15440, doi:10.5194/acpd-10-15417-2010, 2010.
Haynes, J. M., L'Ecuyer, T. S., Stephens, G. L., Miller, S. D., Mitrescu, C., Wood, N. B., and Tanelli, S.: Rainfall retrieval over the ocean with spaceborne W-band radar, J. Geophys. Res., 114, D00A22, doi:10.1029/2008JD009973, 2009.
Haywood, J. M., Osborne, S. R., and Abel, S. J.: The effect of overlying absorbing aerosol layers on remote sensing retrievals of cloud effective radius and cloud optical depth, Q. J. Roy. Meteor. Soc., 130, 779–800, 2004.
Hersey, S. P., Sorooshian, A., Murphy, S. M., Flagan, R. C., and Seinfeld, J. H.: Aerosol hygroscopicity in the marine atmosphere: a closure study using high-time-resolution, multiple-RH DASH-SP and size-resolved C-ToF-AMS data, Atmos. Chem. Phys., 9, 2543–2554, doi:10.5194/acp-9-2543-2009, 2009.
Jiang, H. L., Feingold, G., and Koren, I.: Effect of aerosol on trade cumulus cloud morphology, J. Geophys. Res., 114, D11209, doi:10.1029/2009JD011750, 2009.
Jiang, H. L., Feingold, G., and Sorooshian, A.: Effect of aerosol on the susceptibility and efficiency of precipitation in trade cumulus clouds, J. Atmos. Sci., 67, 3525–3540, 2010.
Lebsock, M. D., Stephens, G. L., and Kummerow, C.: Multi-sensor observations of aerosol effects on warm clouds, J. Geophys. Res., 113, D15205, 2008.
Lohmann, U. and Feichter, J.: Global indirect aerosol effects: a review, Atmos. Chem. Phys., 5, 715–737, doi:10.5194/acp-5-715-2005, 2005.
Lu, M.-L., Sorooshian, A., Jonsson, H. H., Feingold, G., Flagan, R. C., and Seinfeld, J. H.: Marine stratocumulus aerosol-cloud relationships in the MASE-II experiment: precipitation

ACPD
10, 29897–29922, 2010

susceptibility in Eastern Pacific marine stratocumulus, J. Geophys. Res., 114, D24203, doi:10.1029/2009JD012774, 2009.
Masunaga, H., Nakajima, T. Y., Nakajima, T., Kachi, M., Oki, R., and Kuroda, S.: Physical properties of maritime low clouds as retrieved by combined use of tropical rainfall measurement mission microwave imager and visible/infrared scanner: algorithm, J. Geophys. Res., 107, 4083, doi:10.1029/2001JD000743, 2002.
Matsui, T., Masunaga, H., Pielke Sr., R. A., and Tao, W.-K.: Impact of aerosols and atmospheric thermodynamics on cloud properties within the climate system, Geophys. Res. Lett., 31, L06109, doi:10.1029/2003GL019287, 2004.
Matsui, T., Masunaga, H., Kreidenweis, S. M., Pielke Sr., R. A., Tao, W.-K., Chin, M., and Kaufman, Y. J.: Satellite-based assessment of marine low cloud variability associated with aerosol, atmospheric stability, and the diurnal cycle, J. Geophys. Res., 111, D17204, doi:10.1029/2005JD006097, 2006.
McComiskey, A. and Feingold, G.: Quantifying error in the radiative forcing of the first aerosol indirect effect, Geophys. Res. Lett., 35, L02810, doi:10.1029/2007GL032667, 2008.
Partain, P.: Cloudsat ECMWF-AUX auxiliary data process description and interface control document, http://www.cloudsat.cira.colostate.edu/dataICDlist.php?go=list&path=/ECMWF-AUX, 2007.
Pawlowska, H. and Brenguier, J. L.: An observational study of drizzle formation in stratocumulus clouds for general circulation model (GCM) parameterizations, J. Geophys. Res., 108, D15, 8630, doi:10.1029/2002JD002679, 2003.
Platnick, S., King, M. D., Ackerman, S. A., Menzel, W. P., Baum, B. A., Riedi, J. C., and Frey, R. A.: The MODIS cloud products: algorithms and examples from Terra, IEEE T. Geosci. Remote, 41, 459–473, 2003.
Quaas, J., Ming, Y., Menon, S., Takemura, T., Wang, M., Penner, J. E., Gettelman, A., Lohmann, U., Bellouin, N., Boucher, O., Sayer, A. M., Thomas, G. E., McComiskey, A., Feingold, G., Hoose, C., Kristjánsson, J. E., Liu, X., Balkanski, Y., Donner, L. J., Ginoux, P. A., Stier, P., Grandey, B., Feichter, J., Sednev, I., Bauer, S. E., Koch, D., Grainger, R. G., Kirkevåg, A., Iversen, T., Seland, Ø., Easter, R., Ghan, S. J., Rasch, P. J., Morrison, H., Lamarque, J.-F., Iacono, M. J., Kinne, S., and Schulz, M.: Aerosol indirect effects – general circulation model intercomparison and evaluation with satellite data, Atmos. Chem. Phys., 9, 8697–8717, doi:10.5194/acp-9-8697-2009, 2009.
Remer, L. A., Kaufman, Y. J., Tanre, D., Mattoo, S., Chu, D. A., Martins, J. V., Li, R. R.,

ACPD
10, 29897–29922, 2010

Ichoku, C., Levy, R. C., Kleidman, R. G., Eck, T. F., Vermote, E., and Holben, B. N.: The MODIS aerosol algorithm, products, and validation, J. Atmos. Sci., 62, 947–973, 2005.

Rosenfeld, D. and Gutman, G.: Retrieving microphysical properties near the tops of potential rain clouds by multispectral analysis of AVHRR data, Atmos. Res., 34, 259–283, 1994.

Sorooshian, A. and Duong, H. T.: Ocean Emission Effects on Aerosol-Cloud Interactions: Insights from Two Case Studies, Advances in Meteorology, 2010, 301395, doi:10.1155/2010/301395, 2010.

Sorooshian, S., Hsu, K. L., Gao, X., Gupta, H. V., Imam, B., and Braithwaite, D.: Evaluation of PERSIANN system satellite-based estimates of tropical rainfall, B. Am. Meteorol. Soc., 81, 2035–2046, 2000.

Sorooshian, A., Feingold, G., Lebsock, M. D., Jiang, H., and Stephens, G.: On the precipitation susceptibility of clouds to aerosol perturbation, Geophys. Res. Lett., 36, L13803, doi:10.1029/2009GL038993, 2009.

Sorooshian, A., Feingold, G., Lebsock, M. D., Jiang, H., and Stephens, G.: Deconstructing the precipitation susceptibility construct: improving methodology for aerosol-cloud-precipitation studies, J. Geophys. Res., 115, D17201, doi:10.1029/2009JD013426, 2010.

Stevens, B., Feingold, G., Cotton, W. R., and Walko, R. L.: Elements of the microphysical structure of numerically simulated nonprecipitating stratocumulus, J. Atmos. Sci., 53, 980.1006, 1996.

vanZanten, M. C., Stevens, B., Vali, G., and Lenschow, D. H.: Observations of drizzle in nocturnal marine stratocumulus, J. Atmos. Sci., 62, 88–106, 2005.

Wilcox, E. M., Harshvardhan, and Platnick, S.: Estimate of the impact of absorbing aerosol over cloud on the MODIS retrievals of cloud optical thickness and effective radius using two independent retrievals of liquid water path, J. Geophys. Res., 114, D05210, doi:10.1029/2008JD010589, 2009.

Wood, R.: Drizzle in stratiform boundary layer clouds. Part 1: Vertical and horizontal structure, J. Atmos. Sci., 62, 3011–3033, 2005.

ACPD
10, 29897–29922, 2010

Table 1. Aircraft measurement summary of the sensitivity of ACI, χ, and S_o (or S'_o) to the choice of how the aerosol proxy (N_d or N_a), R, and r_e are quantified. The maximum values ("max") are quantified as being the average of the 3 points before/after the maximum value (corresponding to a level flight length of ~350 m). Column-integrated values ("col") represent the vertical integration of leg-mean values of the respective parameter. Cloud-top and base values ("top" and "base") represent the leg-mean value below cloud-top and above cloud base, respectively. N_a is the leg-mean average of particle concentration below cloud-base, as quantified with both a CPC 3010 (D_p>10 nm) and a PCASP (D_p~100 nm–2.6 µm). Bold signify that those points are not statistically significant with 95% confidence based on the student's t-test. Numbers in parentheses next to column and row headers correspond to the overall range of those values (Units: N_d and N_a=# cm^{-3}; r_e=µm; R=mm day^{-1}).

	$N_{d,max}$ (86–407)	$N_{d,col}$ (47–229)	N_a from CPC 3010 (187–1360)	N_a from PCASP (54–424)	$r_{e,max}$	$r_{e,col}$	$r_{e,top}$
			ACI				
$r_{e,max}$ (8.97–14.0)	0.31	0.24	0.22	0.23			
$r_{e,col}$ (8.26–11.2)	0.18	0.15	0.13	0.13			
$r_{e,top}$ (8.34–12.4)	0.21	0.20	0.14	0.16			
	S_o		S'_o			χ	
R_{max} (0.75–8.19)	1.23	1.10	0.88	0.90	4.24	4.16	4.20
R_{col} (0.5–1.60)	0.37	0.44	0.19	0.25	1.31	**0.78**	0.93
R_{base} (0.5–2.75)	0.56	0.67	0.33	0.40	1.82	**1.05**	1.23

ACPD
10, 29897–29922, 2010

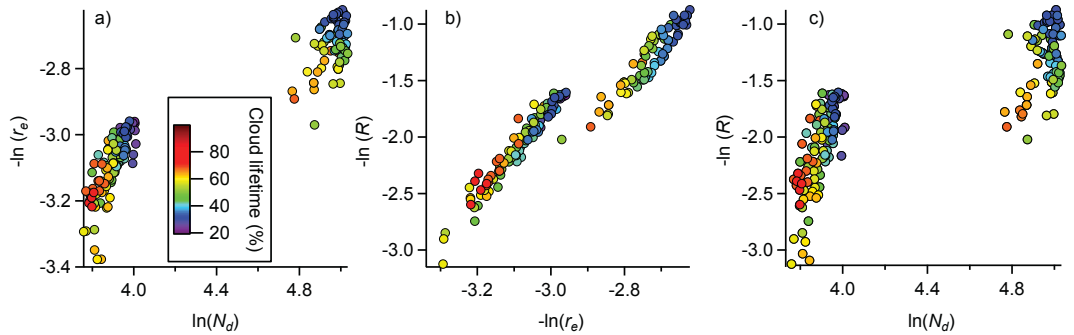

Fig. 1. Large eddy simulation analysis of the effect of cloud lifetime on the quantification of **(a)** $-\frac{\partial \ln r_e}{\partial \ln N_d}\Big|_{LWP}$ (=ACI with N_d in denominator), **(b)** χ, and **(c)** S_o for a representative LWP bin of 800 g m^{-2}. The metric values are taken as slopes of the best fit lines. These data represent values quantified at a spatial resolution of 0.3×0.3 km resolution.

ACPD
10, 29897–29922, 2010

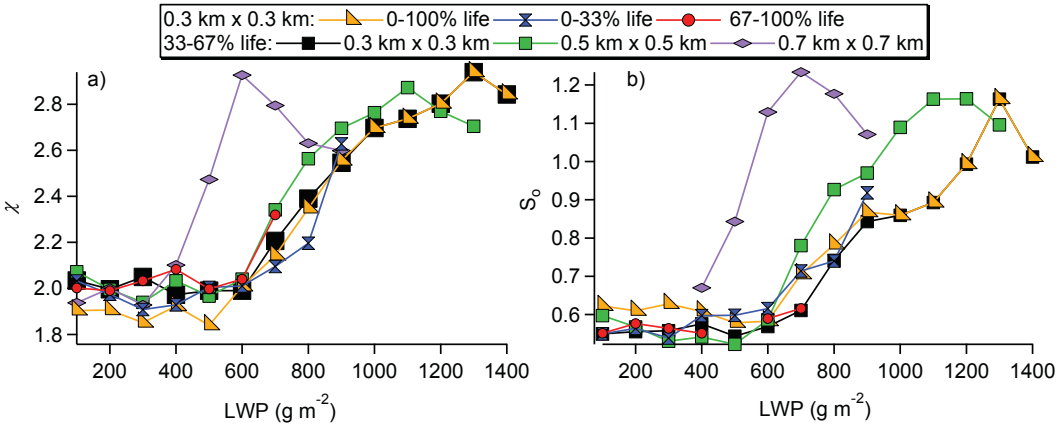

Fig. 2. Large eddy simulation analysis of the dependence of **(a)** χ and **(b)** S_o on LWP, cloud lifetime, and spatial resolution over which data for aerosol and cloud properties were obtained from the LES output.

ACPD
10, 29897–29922, 2010

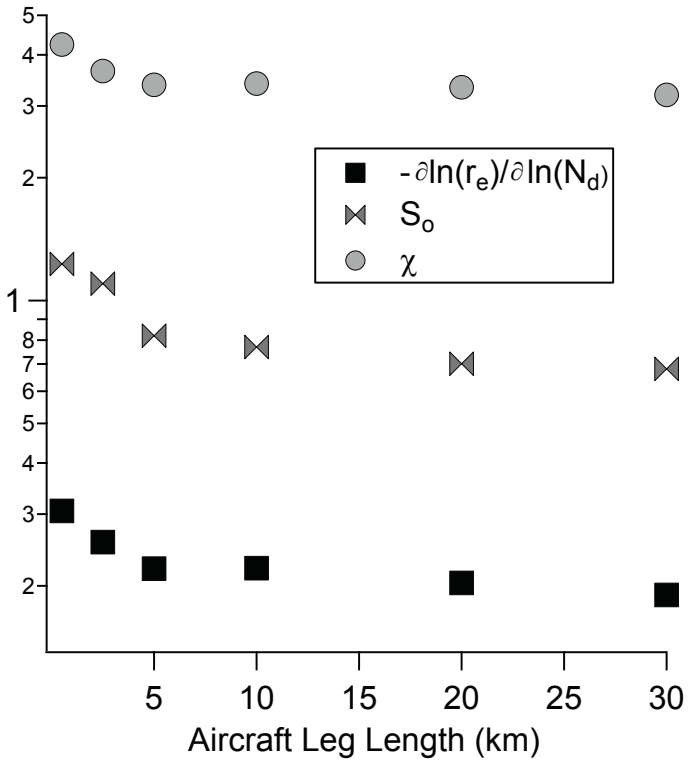

Fig. 3. Aircraft measurements showing the dependence of aerosol–cloud-rain relationships on flight leg length (centered around maximum drop effective radius during a level leg) over which data are analyzed. These data represent stratocumulus clouds off the central coast of California with a LWP range between 31–55 g m^{-2}.

ACPD
10, 29897–29922, 2010

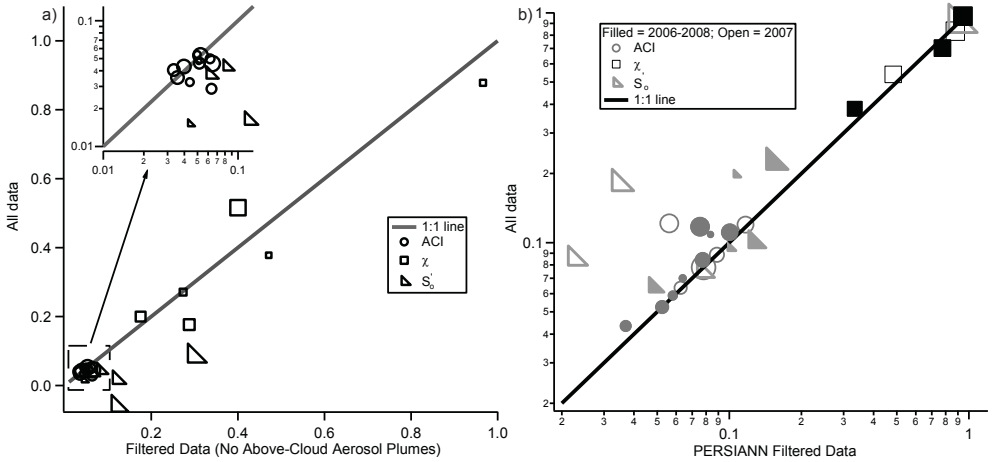

Fig. 4. Satellite data analysis of the sensitivity of aerosol–cloud-rain metrics to above-cloud aerosol plumes and wet scavenging. **(a)** Comparison of ACI, χ, and S_o' with and without above-cloud aerosol plumes off the coast of western Africa. The data represent the time period between June and October 2006. Marker sizes are proportional to LWP (11 LWP bins with up to 10% spacing around bin midpoints (LWP±10%×LWP), which increase in 25 g m^{-2} increments from 50 to 300 g m^{-2}). **(b)** Comparison of ACI, χ, and S_o' with and without filtering of wet scavenging events prior to A-Train overpasses within the same 1°×1° pixel. Marker sizes are proportional to LWP (12 LWP bins with up to 10% spacing around bin midpoints, which include 50 g m^{-2}, 100 g m^{-2}, and up to 1100 g m^{-2} in 100 g m^{-2} increments). The data represent the JJA months for the three year period including 2006–2008 (filled) and 2007 only (open). Only points are reported in both panels that were statistically significant at 95% confidence (based on student's t-test) with and without the data filtering.

ACPD
10, 29897–29922, 2010

Biases in aerosol-cloud-rain interactions

H. T. Duong et al.

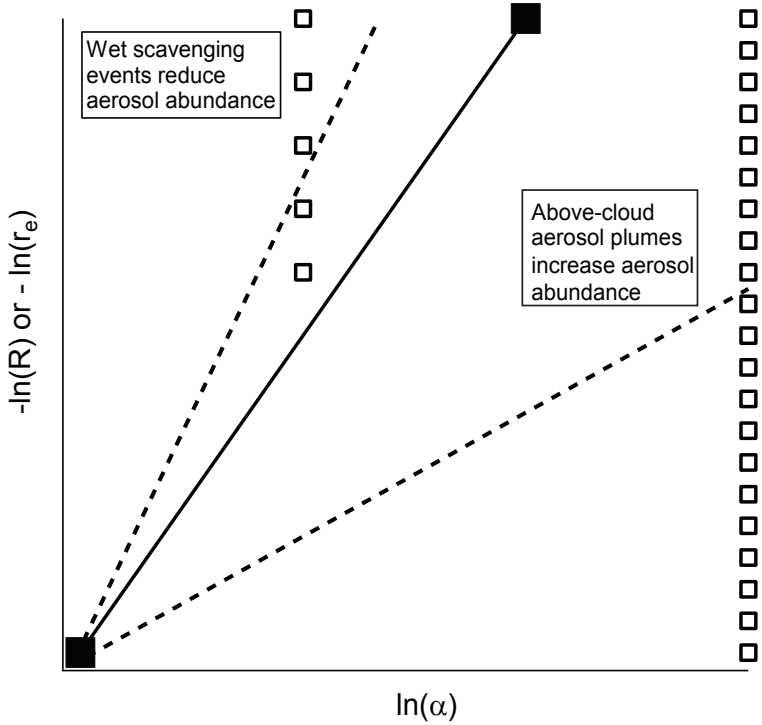

Fig. 5. A visual description of the effect that high and low aerosol concentrations may have on quantification of ACI and S_o' when using satellite data. The thick solid line represents a hypothetical slope when plotting $-\ln(R)$ or $-\ln(r_e)$ versus $\ln(\alpha)$, which corresponds to ACI and S_o', respectively. With above-cloud aerosol plumes, a cluster of points at high levels of $\ln(\alpha)$ will reduce the slope (i.e. lower ACI and S_o'). Low aerosol concentrations as a result of wet scavenging likely will have a greater impact for the most polluted scenes where there is a greater potential to have a reduction in aerosol concentration. This will lead to a higher slope (i.e. higher ACI and S_o'). The χ metric is relatively insensitive to these effects as it avoids the use of retrieved aerosol data.

ACPD
10, 29897–29922, 2010